Posterior Parietal Cortex Regulates Intrinsic Neural Timescales and Attentional Processing in Frontal Eye Field

Orhan Soyuhos[1,2], Tirin Moore[5], Rishidev Chaudhuri[1,3,4], and Xiaomo Chen[1,3,6,*]

[1]Center for Neuroscience, University of California, Davis, Davis, CA, USA
[2]Department of Psychology, University of California, Davis, Davis, CA, USA
[3]Department of Neurobiology, Physiology and Behavior, University of California, Davis, Davis, CA, USA
[4]Department of Mathematics, University of California, Davis, Davis, CA, USA
[5]Department of Neurobiology, Howard Hughes Medical Institute, Stanford University, Stanford, CA, USA
[6]Lead contact
[*]Correspondence: xmch@ucdavis.edu

SUMMARY

Intrinsic neural timescales characterize the dynamics of endogenous fluctuations in neural activity. We measured the intrinsic timescales of frontal eye field (FEF) neurons and examined changes during posterior parietal cortex (PPC) inactivation. FEF neurons exhibit a bimodal distribution of intrinsic timescales, with shorter timescale neurons processing rapid visual information and longer timescale neurons more involved in sustained attentional modulation. PPC inactivation significantly increased intrinsic timescales in both neuron types, with a 15-fold greater increase in shorter timescale neurons. Additionally, PPC inactivation reduced visual and attentional responses, with a stronger effect on attention in longer timescale neurons. This disruption eliminated the correlation between timescales and attentional responses observed in the control condition. Our results provide the first causal evidence that FEF intrinsic timescales depend on long-range projections from PPC, suggesting the presence of at least two network motifs with different timescales that contribute to neuronal dynamics and functional computations within FEF.

KEYWORDS

frontoparietal network, neural circuit, neural timescales, network dynamics, visual attention

INTRODUCTION

Intrinsic neural timescales measure the rate at which intrinsic neural activity is carried over time, reflecting the duration over which endogenous neural activity is influenced by its past independent of external stimuli or specific behavior tasks (Hasson et al., 2015; Murray et al., 2014). Previous research has shown that these timescales vary significantly across different brain regions, highlighting the specialization of each area for various cognitive tasks (Murray et al., 2014). Along the visual hierarchy, early visual regions exhibit shorter intrinsic timescales, whereas higher-order regions show longer timescales. This difference may correspond to their computational functions: early visual areas process rapidly changing visual input, while higher-order regions, like the prefrontal cortex (PFC), maintain goal-relevant information for sustained attention and

working memory. Additionally, within a cortical region, heterogeneity in intrinsic timescales has been shown to reflect the functional specialization of individual neurons (Cavanagh et al., 2020; Wasmuht et al., 2018; Zeraati et al., 2023). Thus, the diversity of these intrinsic timescales across and within regions is considered a fundamental principle for understanding how the brain integrates and segregates information during visual and attentional processing (Wolff et al., 2022).

The variation in intrinsic timescales across cortical areas is believed to be closely associated with both inter- and intra-area connectivity (Wang, 2020). Within a cortical area, the hierarchical organization of timescales is linked to the strength of neural connections, which is shaped by factors such as dendritic spine density in pyramidal neurons (Elston, 2000, 2003; Elston et al., 2011), the expression levels of NMDA and GABA receptor genes (Gao et al., 2020), and the extent of structural and functional connectivity (Hart and Huk, 2020; Fallon et al., 2020; Wasmuht et al., 2018). Computational models also support the connection between neural connectivity and intrinsic timescales, showing that a hierarchy of timescales can emerge naturally from biophysically detailed models (Chaudhuri et al., 2015; Demirtaş et al., 2019). These models suggest that intrinsic timescales arise from a combination of diverse excitatory connection strengths across different regions and long-range connectivity patterns, indicating that neither factor alone is sufficient to predict a region's timescales (Chaudhuri et al., 2015, 2014; Litwin-Kumar and Doiron, 2012). Despite the strong correlation and evidence from computational models, the direct causal link between structural connectivity and intrinsic timescales remains unexplored.

In the primate brain, the frontal eye field (FEF) and the posterior parietal cortex (PPC) are key regions within the frontoparietal attention network (Boshra and Kastner, 2022), with the PPC situated earlier and the FEF located later in the visual hierarchy (Markov et al., 2011). Both areas are involved in representing stimulus-driven and goal-directed visual attention (Boshra and Kastner, 2022; Moore and Zirnsak, 2017). Importantly, the FEF has been shown to be a critical source of control for goal-directed attention (Moore and Fallah, 2001; Moore and Armstrong, 2003). More recently, our previous research demonstrated a causal role of the PPC in regulating stimulus-driven attentional representation in the FEF and influencing behavior (Chen et al., 2020). Anatomically, the FEF and oculomotor areas within the PPC, such as the lateral intraparietal area (LIP), are heavily reciprocally connected (Lynch and Tian, 2006). This interaction between the FEF and PPC is believed to play a crucial role in various cognitive functions, including visual attention (Murray et al., 2017; Hart and Huk, 2020). Additionally, the FEF receives direct projections from most of the functionally defined areas within the visual cortex (Schall et al., 1995) and sends feedback projections to the majority of the visual cortex (Schall et al., 1995; Stanton et al., 1995). Therefore, the FEF is thought to act as a proxy for the prefrontal cortex's communication with visual areas through these anatomical connections.

In this study, we investigate how the intrinsic timescales of individual FEF neurons, measured during the pre-trial fixation period, relate to their functional specialization in stimulus-driven visual attention. We also explore the dependence of these timescales on long-range connections from the PPC. Our findings reveal that FEF neurons exhibit a bimodal distribution of intrinsic timescales: neurons with shorter timescales are more involved in rapid visual processing, while those with longer timescales are more engaged in sustained attentional modulation. Furthermore, PPC inactivation selectively increases the intrinsic timescales of shorter timescale neurons while reducing the attentional responses of longer timescale neurons. As a result, PPC inactivation disrupts FEF neural dynamics, revealing for the first time the causal role of long-range connectivity between these regions in regulating FEF neural timescales. PPC inactivation also disrupts attentional processing in the FEF, underscoring the role of the parietal cortex in modulating salience signals within the FEF. These findings highlight the importance of long-range connectivity in regulating both neural dynamics and attentional processes across these regions.

RESULTS

We recorded spiking activity within the FEFs using multichannel microelectrodes (see *STAR Methods*) while the monkey was performing a passive viewing task (Figure 1A). Within each trial, we measured the spiking responses to either a single visual probe (Single) or a unique stimulus (Pop-out) (Figure 1B). Additionally, we reversibly inactivated the PPC of two behaving monkeys (J and Q) via cryoloops that were chronically implanted within the intraparietal sulcus (IPS) and compared the spiking activity within the FEFs with parietal inactivation (Inactivation condition) and without parietal inactivation (Control condition). In total, 400 single- and multi-unit spiking activities were recorded from 192 FEF sites over 11 recording sessions (Experimental Procedures).

Two Distinct Neural Timescales in FEF Neurons

We first analyzed the intrinsic neural timescales of FEF neurons across two monkeys under PPC control and inactivation conditions. We calculated the autocorrelation values for each neuron using endogenous fluctuations of spiking activity over the baseline period before stimulus presentation (Figure 1C). We then fitted a single exponential decay function to these autocorrelation values to determine the intrinsic neural timescales (τ) for each neuron (Figure 1D) (Murray et al., 2014). A relatively longer τ indicated that intrinsic neural activity was sustained over extended periods with a stable firing pattern, whereas a shorter τ signified more transient activity characterized by a dynamic baseline firing pattern. We used pseudo-R-squared values (Figure 1S) to quantify the goodness of fit between our model and the observed data. Overall, the exponential function matched well with the observed data (mean $R^2 = 0.78$; Monkey J $= 0.73$; Monkey Q $= 0.83$). We excluded 20 units with R-squared values smaller than 0.3, ending up with 380 neurons for the control condition.

The probability density of the timescale values for FEF neurons exhibited a bimodal distribution (Figure 2). This is confirmed by several statistical tests, including the most recent bimodality test, the Excess Mass Test (Ameijeiras-Alonso et al., 2019). This test indicated significant bimodality with an overall value of 0.072 ($p < 2.2 \times 10^{-16}$), with values for Monkey Q at 0.091 ($p < 2.2 \times 10^{-16}$) and Monkey J at 0.072 ($p < 1.6 \times 10^{-2}$). We then divided the neurons into two shorter and longer τ groups using the global minimum of their kernel density estimate (60.95 ms), derived from the combined distribution across both monkeys. These global minimums were also consistent across individual monkeys (Monkey J = 60.51 ms and Monkey Q = 59.33 ms) (Figure 2B). As a result, neurons with shorter timescales exhibited a fast decay rate ($N = 168$, Mean = 27.34 ms), whereas neurons with longer timescales showed a slower decay rate in their autocorrelation values during the baseline period ($N = 212$, Mean = 102.64 ms). Similar distributions were observed for both Monkey J and Q (Shorter τ neurons: Monkey J = 28.17 ms and Monkey Q = 26.71 ms; Longer τ neurons: Monkey J = 104.78 ms and Monkey Q = 100.73 ms).

Intrinsic Neural Timescales Correlate With Functional Selectivity in FEF Neurons

Next, we examined the relationship between intrinsic neural timescales and the functional response properties of individual units. A visual index was used to quantify the increase in neuronal response by comparing a single stimulus inside versus outside the receptive field (RF). Similarly, an attention index was used to quantify response enhancement by comparing unique stimuli inside versus outside the RFs. We further divided the neuronal response into transient (50–200 ms) and sustained (200–500 ms) periods following stimulus onset. This allowed us to

calculate a transient visual index, sustained visual index, transient attention index, and sustained attention index to quantify the functional response properties of each unit (see *STAR Methods*).

We used multiple linear regression analysis to assess the specific relationships between intrinsic neural timescales and both visual and attentional selectivity indices (transient or sustained), while controlling for the influence of other predictors. For visual responses, our results revealed a significant negative association between intrinsic timescales and transient visual selectivity indices (Permutation test: $p < 2 \times 10^{-4}$, $\beta = -73.98$), and no significant relationship between timescales and sustained visual selectivity indices (Permutation test: $p = 0.24$, $\beta = 26.32$). For attentional responses, there is a significant positive relationship between intrinsic timescales and sustained attentional selectivity indices (Permutation test: $p < 9 \times 10^{-4}$, $\beta = 77.18$), as well as a significant negative relationship between intrinsic timescales and transient attentional selectivity indices (Permutation test: $p < 2.05 \times 10^{-2}$, $\beta = -53.98$) (Figure 3A). These findings demonstrate a clear correlation between individual FEF neurons' intrinsic timescales and their visual and attentional response properties.

Given the correlations between visual and attentional response properties and the intrinsic timescales of FEF neurons, we next asked whether visual and attentional responses differ between shorter and longer timescale neurons (Figure 3B). First, we compared the visual and attention indices between shorter and longer τ neurons. The distributions for transient visual (Cramer-von Mises test, $p < 9.99 \times 10^{-4}$) and transient attention indices (Cramer-von Mises test, $p < 1.60 \times 10^{-2}$) differed significantly between the two groups, whereas sustained indices were not significantly different for either visual (Cramer-von Mises test, $p = 0.178$) or attention at the individual level (Cramer-von Mises test, $p = 0.924$) (Figure 3C). Next, we compared the amount of visual and attentional information that shorter and longer τ neurons possessed at the population level and performed population decoding analysis to predict the location (In-RF vs. Out-RF) of either the single or unique stimuli. We generated neuron-dropping curves (NDCs) (Lebedev, 2014; Pettine et al., 2019; Wessberg et al., 2000) across varying population sizes. Both groups have high decoding performance and are above chance level for all population sizes (Figure 3D-E). We then fit a saturation function to these NDCs and compared the fit parameters for saturation rate and asymptote between shorter and longer τ populations.

For the transient visual response, the NDC for shorter τ neurons had a significantly greater saturation rate than that of longer τ neurons (Wilcoxon rank-sum test: $p = 4.90 \times 10^{-7}$, median $B = 0.323$ [CI: $0.306, 0.356$] for shorter τ, median $B = 0.252$ [CI: $0.231, 0.270$] for longer τ). For the attentional response, the NDC for longer τ neurons had a significantly higher saturation rate than that of shorter τ neurons during the transient period (Wilcoxon rank-sum test: $p = 3.45 \times 10^{-2}$, median $B = 0.044$ [CI: $0.040, 0.047$] for longer τ, median $B = 0.041$ [CI: $0.039, 0.044$] for shorter τ) and also a significantly higher asymptote during the sustained period (Wilcoxon rank-sum test: $p = 1.02 \times 10^{-5}$, median $C = 0.993$ [CI: $0.992, 0.994$] for longer τ, median $C = 0.989$ [CI: $0.986, 0.991$] for shorter τ) (Figure 3E). To outline these differences, we compared the number of neurons needed to achieve equivalent performance levels in both populations. For the sustained attentional response, the longer τ neurons achieved an asymptotic performance of 0.993 with only 82 units, whereas shorter τ neurons achieved an equivalent performance with 103 units, an increase of approximately 26%. For the transient visual response, the shorter τ neurons achieved an asymptotic performance of 1 with only 55 units, while an equivalent performance was achieved by the longer τ neurons with 83 units, an increase of approximately 51%.

In summary, consistent with the multiple linear regression analysis, our results showed that neurons with faster intrinsic timescales (shorter τ) exhibit stronger transient visual responses, while neurons with slower timescales (longer τ) display more robust sustained attentional responses.

PPC Inactivation Selectively Increases the Intrinsic Timescales of Shorter Timescales Neurons in FEF

We then investigated the effects of PPC inactivation on intrinsic neural timescales in the FEF. Figure 4A illustrates the changes in timescales for several example neurons during PPC inactivation. These representative neurons exhibited increased timescales and a more stable firing pattern during the initial baseline period. We further analyzed the changes in timescales across the entire population of FEF neurons. We found a significant increase in their timescales following PPC inactivation (Wilcoxon signed-rank test: $p < 5.09 \times 10^{-13}$, effect size $= 0.432$, mean $= 84.43$ ms, median $= 94.92$ ms for inactivation vs. mean $= 69.89$ ms, median $= 73.14$ ms for control) (Figure 4B). This increase in timescales was evident for both monkeys (Wilcoxon signed-rank test: $p = 3.02 \times 10^{-2}$, effect size $= 0.19$ for Monkey J; $p < 4.00 \times 10^{-15}$, effect size $= 0.63$ for Monkey Q). As a result, we observed a substantial increase (29.52%) in the number of longer τ neurons ($N_{\text{Control}} = 210$; $N_{\text{Inactivation}} = 272$) and a corresponding decrease (38.27%) in the number of shorter τ neurons during PPC inactivation ($N_{\text{Control}} = 162$; $N_{\text{Inactivation}} = 100$) (Figure 4C).

We further examined the changes in timescales separately for shorter τ neurons and longer τ neurons (Figure 4D). We found that the increase in timescales is more pronounced in neurons with shorter timescales compared to those with longer timescales (Wilcoxon rank-sum test: $p < 8.64 \times 10^{-9}$, effect size $= 0.35$) (Figure 4E). Although there is a significant increase in timescales for both shorter τ neurons (Wilcoxon signed-rank test: $p < 1.02 \times 10^{-13}$, effect size $= 0.67$) and longer τ neurons (Wilcoxon signed-rank test: $p = 7.79 \times 10^{-3}$, effect size $= 0.21$), these changes in shorter τ neurons were 15-fold greater than the changes in longer τ neurons (Shorter τ neurons: Δmean $= 30$ ms, Δmedian $= 19$ ms; Longer τ neurons: Δmean $= 2$ ms, Δmedian $= 4$ ms). These results indicate a selective increase in timescales among FEF shorter τ neurons during PPC inactivation. Therefore, PPC inactivation has a stronger impact on the neuronal dynamics of shorter τ neurons compared to those of longer τ neurons.

PPC Inactivation Selectively Modulates Attention Processing in FEF Neurons with Longer Timescales

Finally, we investigated whether the relationship between neuronal timescales and functional properties of FEF neurons depends on long-range projections between PPC and FEF. We employed multiple linear regression analysis to assess the correlation between intrinsic neural timescales and both visual and attentional selectivity indices during control and inactivation conditions (Figure 5A). Our analysis revealed that the correlation between intrinsic timescales and attentional modulation relies on PPC-FEF connections. Specifically, the significant negative association between transient attentional selectivity and intrinsic timescales in the control condition (Permutation test: $p = 0.02$, $\beta = -53.98$) was no longer significant after PPC inactivation (Permutation test: $p = 0.63$, $\beta = -12.45$). Similarly, the positive association between sustained attentional selectivity and intrinsic timescales under control conditions (Permutation test: $p < 9 \times 10^{-4}$, $\beta = 77.18$) became non-significant following inactivation (Permutation test: $p = 0.21$, $\beta = -32.12$). For visual responses, while there was a significant negative correlation between intrinsic timescales and transient visual selectivity in the control condition (Permutation test: $p < 2 \times 10^{-4}$, $\beta = -73.98$), this correlation weakened but persisted after inactivation (Permutation test: $p = 0.03$, $\beta = -44.83$). No significant relationship was found between intrinsic timescales and sustained visual selectivity in either condition (Permutation test: $p = 0.24$, $\beta = 26.32$). Thus, the correlation between intrinsic timescales and visual responses weakened but persisted after PPC inactivation, while PPC inactivation completely eliminated the relationship between neural timescales and attentional responses.

Similar results were observed when comparing individual changes (Δ) in visual and attention indices between shorter and longer τ neurons (Figure 5B). The distributions of changes differed significantly for visual transient (Cramer-von Mises test: $p = 2.60 \times 10^{-2}$) and attention sustained responses (Cramer-von Mises test: $p = 1.20 \times 10^{-2}$), with the largest change observed in attention sustained indices for the longer τ neurons (median $= -0.17$). No significant differences were found for visual sustained (Cramer-von Mises test: $p = 0.06$) or attention transient responses (Cramer-von Mises test: $p = 0.62$).

Next, we examined whether these changes could be observed at the population level and whether they differ between shorter and longer τ groups (Figure 5C-D). For visual-decoding performance, as measured by AUC (area under the curve exceeding the chance level) of NDCs, both shorter and longer τ neurons showed slight but significant decreases during the transient period (Δ: -0.31% for shorter τ, Wilcoxon signed-rank test: $p = 4.64 \times 10^{-12}$; -0.67% for longer τ, Wilcoxon signed-rank test: $p = 8.46 \times 10^{-16}$), with longer τ neurons exhibiting a larger decrease (Wilcoxon rank-sum test: $p = 5.94 \times 10^{-8}$). During the sustained period, the Δ was -0.31% for shorter τ (Wilcoxon signed-rank test: $p = 1.12 \times 10^{-3}$) and -1.97% for longer τ (Wilcoxon signed-rank test: $p = 9.46 \times 10^{-18}$), again showing a more pronounced decrease in longer τ neurons (Wilcoxon rank-sum test: $p = 1.01 \times 10^{-20}$). In contrast, attention-decoding performance exhibited larger reductions. Shorter τ neurons showed a Δ of 21.50% in transient attention performance (Wilcoxon signed-rank test: $p = 3.96 \times 10^{-18}$) and 12.84% in sustained attention (Wilcoxon signed-rank test: $p = 3.96 \times 10^{-18}$), while longer τ neurons showed a Δ of 20.07% in transient (Wilcoxon signed-rank test: $p = 3.96 \times 10^{-18}$) and 23.28% in sustained attention (Wilcoxon signed-rank test: $p = 3.96 \times 10^{-18}$). Although both groups experienced reductions, longer τ neurons showed significantly greater decreases in sustained attention performance (Wilcoxon rank-sum test: $p = 1.23 \times 10^{-28}$) (Figure 5E-F).

To further quantify these differences, we compared changes (Δ) in saturation rate and asymptote between shorter and longer τ populations. For saturation rate, significant differences were observed in visual sustained (Wilcoxon rank-sum test: $p < 7.64 \times 10^{-6}$) and attention sustained (Wilcoxon rank-sum test: $p < 4 \times 10^{-7}$) conditions, with shorter τ neurons showing smaller reductions (Δ median: -0.006 vs. -0.046 for visual sustained, and Δ median: -0.017 vs. -0.032 for attention sustained). In the attention transient condition, shorter τ neurons also showed smaller reductions compared to longer τ neurons (Wilcoxon rank-sum test: $p < 3.38 \times 10^{-2}$, Δ median: -0.016 vs. -0.020), while no significant difference was found in the visual transient condition (Wilcoxon rank-sum test: $p = 0.1$). For asymptote, significant differences were seen across all conditions, though the visual differences were smaller (for visual transient, Wilcoxon rank-sum test: $p < 1.86 \times 10^{-2}$; for visual sustained, Wilcoxon rank-sum test: $p < 4.13 \times 10^{-4}$). In contrast, attention-decoding performance showed larger differences: shorter τ neurons exhibited a smaller reduction in attention transient (Wilcoxon rank-sum test: $p < 4.52 \times 10^{-2}$, Δ median: -0.035 vs. -0.018) and attention sustained (Wilcoxon rank-sum test: $p < 3.05 \times 10^{-2}$, Δ median: -0.018 vs. -0.023).

In summary, while PPC inactivation weakened the relationship between intrinsic timescales and visual responses, it selectively diminished the relationship between intrinsic timescales and attentional responses. Particularly, PPC inactivation has a more pronounced effect on the attentional response of longer τ neurons at both single and population levels.

DISCUSSION

We investigated the intrinsic neural timescales within the FEF and discovered for the first time a bimodal distribution, suggesting the presence of two distinct neuronal populations specialized for different functional roles in visual processing and attention. Specifically, neurons with shorter

τ are crucial for rapid visual processing, exhibiting strong transient responses to visual stimuli. In contrast, neurons with longer τ contribute to sustained attentional modulation in response to salient stimuli. Notably, inactivation of the PPC selectively increased the intrinsic timescales of neurons with shorter τ during task free epoch and disrupted attentional processing in neurons with longer τ in response to salient stimuli. These findings provide the first causal evidence for the critical role of PPC-FEF connectivity in modulating neural dynamics and functional specialization within the FEF during stimulus-driven attention.

Functional Segregation and Neuronal Properties within the FEF

Along the visual hierarchy, it is well-established that early visual regions exhibit shorter intrinsic timescales, whereas higher-order regions show longer timescales (Murray et al., 2014; Hasson et al., 2015). Our results extend these findings by investigating the diversity of intrinsic timescales within the frontal eye field (FEF), a critical source of control for goal-directed attention (Moore and Fallah, 2001; Moore and Armstrong, 2003). We found that the intrinsic timescales of FEF neurons exhibit a bimodal distribution, reflecting functional segregation within the FEF. Consistent with the hierarchical organization of cortical processing, we observed that FEF neurons with shorter intrinsic timescales (τ) are optimized for the rapid processing of visual stimuli. These neurons likely receive feedforward input from the posterior parietal cortex (PPC) and have weak local recurrent structures (Murray et al., 2017) (Figure 6A), facilitating quick reactions to environmental changes and playing a crucial role in transient visual sensitivity. Conversely, FEF neurons with longer intrinsic timescales are more involved in maintaining attention on salient stimuli over time, likely forming reciprocal connections with the PPC during sustained attention responses (Hart and Huk, 2020) and having strong recurrent structures (Murray et al., 2017) (Figure 6B). They integrate information over extended periods, supporting the robustness of sustained attention and filtering out distractions. In addition to stimulus-driven sustained attention, these neurons may play a key role in various higher-order cognitive processes, including goal-directed attention and working memory (Murray et al., 2014; Wasmuht et al., 2018; Cavanagh et al., 2020; Zeraati et al., 2023). This observed division of labor among FEF neurons highlights intrinsic temporal dynamics as a key factor in functional specialization, enabling efficient management of both immediate visual input processing and the maintenance of attention over time.

Effects of PPC Inactivation on FEF Are Context Dependent

Our results demonstrate that PPC inactivation has a selective impact on FEF neurons with shorter and longer intrinsic τ, depending on the task epoch. During the resting state prior to visual stimulus presentation, we observed that inactivation of the PPC selectively increased the intrinsic timescales of neurons with shorter τ. Given the hypothesized feedforward role of shorter τ neurons, our results suggest that the intrinsic activity during this epoch is largely driven by feedforward input from the PPC in preparing for immediate visual processing. When the PPC was inactivated, these feedforward connections were disrupted, leading to a larger increase in the intrinsic timescales of neurons with shorter τ. This selective increase suggests that, without the influence of the PPC, the fast dynamics of these neurons slow down. This slower dynamic can be driven by two factors: first, the removal of input from faster dynamic PPC neurons; and second, the recruitment of these neurons by longer τ neurons with strong recurrent structures.

During the sustained response period, PPC inactivation led to a significant disruption in attentional processing, particularly in neurons with longer τ. The observation that longer τ neurons show higher attentional selectivity shows that they play a significant role in attentional modulation. Furthermore, the selective reduction of this high attention selectivity suggests that this

processing depends on PPC input, possibly through reciprocal interactions between the FEF and PPC (Figure 6B). These feedback loops might be critical for maintaining attention on salient stimuli over extended periods, highlighting the critical role of the PPC in stimulus-driven attention processing (Chen et al., 2020).

Overall, these findings suggest that while neurons with shorter τ are primarily influenced by the PPC through feedforward mechanisms during resting state and rapid visual processing, neurons with longer τ rely on reciprocal feedback between PPC and FEF to maintain sustained attention response.

Implications for Neural Circuit Models

We provide empirical evidence supporting computational models that link intrinsic timescales to network connectivity and hierarchical processing. Specifically, the modulation of FEF intrinsic timescales by PPC inputs indicates a dependence of FEF temporal properties on long-range connectivity. This dependency suggests that inter-areal interactions play an instrumental role in shaping the temporal dynamics of local circuits. These results highlight the importance of incorporating both local synaptic architecture and inter-areal connectivity patterns into computational neural circuit models to more accurately represent the complexity of cortical dynamics (Chaudhuri et al., 2015).

Moreover, our findings suggest that intrinsic timescales not only differ across cortical areas along the visual hierarchy (Murray et al., 2014) but also exhibit notable heterogeneity within a single brain region such as the FEF, similar to the variability reported in area V4 (Zeraati et al., 2023). This intra-regional variability in temporal dynamics likely reflects a functional specialization among distinct neuron populations, which could underpin different forms of attention processing, such as rapid responses to transient stimuli versus sustained engagement during attentional tasks. Such functional specialization is essential for efficient visual and attentional processing, enabling the brain to adaptively allocate resources according to the temporal demands of diverse stimuli.

These insights suggest that future studies employing large-scale recordings, combined with targeted manipulations, are crucial to further reveal the division of labor between different brain regions as well as the specialized roles of functional neuron classes within distributed attention networks. This understanding will pave the way for a more nuanced view of attentional control, revealing how intrinsic timescales contribute to both within-region and network-wide dynamics that underlie adaptive cognitive functions.

Conclusion

Our study demonstrates that the PPC plays a crucial role in regulating intrinsic neural timescales and attentional processing within the FEF during stimulus-driven attention. The functional diversity within the FEF, characterized by two distinct neuronal populations with different timescales, facilitates both rapid visual processing and sustained attention to salient stimuli. The selective modulation of intrinsic timescales by PPC input underscores the importance of long-range connectivity in shaping neural dynamics and cognitive functions. These novel findings advance our understanding of the neural mechanisms underlying stimulus-driven attention and provide a foundation for future research exploring the dependence and interplay between intrinsic timescales, connectivity, and cortical processing in the dorsal attention network.

STAR METHODS

Key Resources Table

REAGENT.or.RESOURCE	SOURCE	IDENTIFIER
Experimental Models: Organisms/Strains		
Macaca mulatta	Davis Primate Center	N/A
Software and Algorithms		
R version 4.4.1	R Foundation	https://www.r-project.org/
Python 3.8.18	Python Software Foundation	https://www.python.org/
Offline Sorter, Version 3.0		
Data Acquisition	Plexon	https://plexon.com/products/offline-sorter/
OmniPlex System	Plexon	https://plexon.com/products/omniplexd-neural-data-acquisition-system-1/
Other		
SR Research Eyelink Eye Tracker, Eyelink 1000 Plus	Eyelink	http://www.sr-research.com

Resource Availability

Lead Contact

Requests for further information and resources should be directed to and will be fulfilled by the lead contact, Xiaomo Chen (xmch@ucdavis.edu).

Data and Code Availability

The datasets and code supporting the current study have not been deposited in a public repository due to their volume and complexity but will be made available by the lead contact (X.C.) upon request.

Experimental Model and Subject Details

All experimental procedures followed the guidelines set by the National Institutes of Health Guide for the Care and Use of Laboratory Animals, the Society for Neuroscience Guidelines and Policies, and the Stanford University Animal Care and Use Committee. The experiments involved two healthy male rhesus macaques (*Macaca mulatta*): monkey Q (16 kg) and monkey J (17 kg). The number of animals used aligns with typical practices for neurophysiological studies involving non-human primates.

Method Details

Experimental Procedures

The details of the surgical procedures and neurophysiological recordings have been previously reported by Chen et al. (2020). In summary, two monkeys (Q, 16 kg; J, 17 kg) performed visual sensitivity and saliency-driven attention tasks under PPC-inactivation and control conditions while we monitored neural activity in the FEF (Figure 1A). Each trial began with an initial central fixation period (1x1 dva) of 500 ms on a gray background (60 cd/m²), with the last 300 ms serving as the baseline period. Following this, the monkeys were presented with either a single stimulus or a pop-out stimulus for 500 ms while continuing to fixate at the center (Figure 1B). In the single stimulus trials, a red or green square stimulus (7x7 dva) was displayed at one of 24 locations on a 6x4 grid (75x45 dva). In the pop-out trials, a square stimulus was placed at each location, with one square's color differing from the others (red vs. green). Pop-out trials elicited attentional responses due to competing stimuli, whereas single stimulus trials assessed the visual sensitivity of a given neuron in the absence of competing stimuli. After stimulus offset, the monkeys continued fixating for an additional 500 ms to receive a reward (Figure 1C).

Neurophysiological Recording of FEF

The recording locations within the right FEF were identified by eliciting short-latency saccadic eye movements using biphasic current pulses ($\leq$50 μA; 250 Hz; 0.25 ms duration), in line with methods from previous studies (Bruce et al., 1985). Neural activity was recorded using 16 or 32-channel linear array electrodes (V and S-Probes, Plexon, Inc.), with contacts spaced 150 μm apart. These electrodes were inserted into the cortex via a hydraulic microdrive (Narishige International). Neural signals were referenced to a nearby stainless steel guide tube positioned near the electrode contacts. The signal used for spike detection was filtered with a 4-pole Bessel high-pass filter at 300 Hz and a 2-pole Bessel low-pass filter at 6000 Hz, and sampled at 40 kHz. Initial classification of extracellular waveforms into single neurons or multi-units was performed online via template matching, with offline sorting subsequently verified using Plexon systems. In total, we recorded spike timestamps from 400 neural units in the FEF across the two monkeys.

Reversible Inactivation of PPC

In each monkey, a pair of stainless steel cryoloops was implanted in the intraparietal sulcus (IPS) of the right hemisphere. These cryoloops were custom-designed to fit the contours of the IPS and fill the sulcus. The IPS was cooled by circulating chilled methanol through the loop tubing, with the temperature closely monitored and maintained within 1℃ of the target value by adjusting the methanol flow rate. A stable loop temperature of approximately 5℃ was reached within 5–10 minutes after the cooling process began, and the brain's normal temperature was restored within about 2 minutes post-cooling. Temperatures around 5℃ in the loop have been shown to effectively suppress neuronal activity in the underlying cortex (Lomber and Payne, 2000). During the experimental sessions, inactivation periods lasted 30 to 60 minutes each. Neurophysiological data were first collected during a control block, followed by an inactivation block across eight sessions. In six additional sessions, data collection followed two consecutive sets of control and inactivation phases (control-inactivation-control-inactivation), allowing the examination of potential block order effects. The success of PPC inactivation on behavior was evaluated in separate sessions using double-target choice tasks and free viewing of natural images (Chen et al., 2020).

Computation of Intrinsic Neural Timescales

We analyzed neural activity from 400 neural units in the FEF across two monkeys. Each unit's activity was recorded as spike timestamps, which were binned into 10 ms intervals to calculate spike counts for each trial. To normalize the spike counts at each time bin across all trials, we subtracted the mean firing rate of each time bin from the spike count in that bin. This step helped isolate the intrinsic temporal dependencies of the neuron's firing pattern, independent of its overall firing rate. We then performed autocorrelation analysis on the 300 ms baseline windows of each trial to compute the sum of products of spike count values against themselves at various lags for each neuron. The autocorrelation values at each lag were normalized by the value at zero lag, standardizing the results relative to the maximum observed autocorrelation. The resulting autocorrelation values were then averaged across trials for a given neuron, displaying a characteristic exponential decay, decreasing progressively from lower to higher time lags.

We then fitted a single exponential decay function to these averaged autocorrelation values and calculated the decay time constants for each neuron, representing their intrinsic neural timescales (Figure 1D). Importantly, a subset of neurons displayed significantly low autocorrelation values at short time lags, suggesting the presence of refractory periods or negative adaptation, as reported in previous studies (Cavanagh et al., 2016; Murray et al., 2014; Wasmuht et al., 2018). Therefore, the fitting procedure was started at the time lag—excluding the zeroth lag where autocorrelation equals one—where the mean autocorrelation reached its maximum value. For the curve fitting, we used the Trust Region Reflective algorithm. The model used for the fitting process is given by the equation:

$$f(x) = A \cdot \left(e^{-\frac{x}{\tau}} + B\right) \tag{1}$$

where x is the time lag, τ represents the intrinsic timescale, A is the amplitude of the decay, and B is included to adjust for baseline shifts, addressing the influence of intrinsic neural timescales that extend beyond the measurement window.

To establish an objective criterion for the goodness of fit, we calculated pseudo-R^2 values for nonlinear fitting based on the proportion of the total variance explained by the exponential decay function. We found that 5% of units had pseudo-R^2 values below 0.3, indicating a poor fit. Additionally, 6.5% of units fell within the range of 0.3 to 0.5, representing a moderate fit, and 13% of units had values between 0.5 and 0.7, suggesting a good fit. The majority, 75.5% of units, demonstrated values ranging from 0.7 to 1.0, indicating a strong to perfect model fit (Figure S1). Neurons with pseudo-R^2 values below 0.3 were excluded from further analysis, resulting in a remaining sample of 380 neural units for the control condition and 385 neural units for the inactivation condition.

Mode testing of Intrinsic Neural Timescales

To investigate the distribution of intrinsic neural timescales in the FEF, we applied several statistical tests using the mode test function from the multimode R package (Ameijeiras-Alonso et al., 2021). Each test was chosen for its ability to highlight different aspects of distribution modality. We used the Hall and York Critical Bandwidth Test (Hall and York, 2001), which refines bandwidth selection in kernel density estimation to improve the detection of subtle multimodal patterns. The Fisher and Marron Cramer-von Mises Test (Fisher and Marron, 2001) was applied for its sensitivity in capturing subtle features like shoulder modes by assessing how well the empirical distribution function fits a hypothesized unimodal function using the Cramer-von Mises statistic. Additionally, the Hartigan and Hartigan Dip Test (Hartigan and Hartigan, 1985), a nonparametric test, was employed to detect multimodality without assuming a specific distribution form by measuring the maximum difference between the empirical distribution and its

best-fitting unimodal distribution. Lastly, we used the Ameijeiras-Alonso et al. Excess Mass Test (Ameijeiras-Alonso et al., 2019), which employs the excess mass criterion for mode detection, offering a robust method particularly suited for multidimensional datasets with high noise levels. All tests provided complementary results, and we reported the findings from the most recent method using the Excess Mass Test (Ameijeiras-Alonso et al., 2019).

Calculation of Visual and Attention Indices

We measured the receptive field of each neuron by analyzing their neural responses to a single stimulus presented in each of 24 locations. For those locations where a neuron's firing rate exceeded 95% of its maximum response, we included them within the neuron's receptive field. In contrast, the four locations in the far-right column of the visual field were considered outside the receptive field, as they are ipsilateral to the recording site. Following this, we computed visual indices for each neuron, reflecting the neural activity during transient (50-200 ms) and sustained (200-500 ms) periods for both single and pop-out stimulus trials. These indices were calculated based on the average differential spike rate when stimuli were presented within versus outside the neuron's receptive field (In-RF vs. Out-RF; Figure 1B), normalized by their sum.

$$\text{Visual index}_{i,\text{type, period}} = \frac{\overline{\text{In-RF}}_{i,\text{type, period}} - \overline{\text{Out-RF}}_{i,\text{type, period}}}{\overline{\text{In-RF}}_{i,\text{type, period}} + \overline{\text{Out-RF}}_{i,\text{type, period}}} \tag{2}$$

Here, i represents each neuron, 'type' refers to single or pop-out trials, and 'period' denotes transient or sustained periods. We computed four visual indices corresponding to transient and sustained visual sensitivity as well as attentional responses. Additionally, we calculated the mean baseline firing rate of each neuron to account for inter-neuron differences.

Multiple Linear Regression Analyses

We conducted multiple regression analyses to determine the individual contributions of each variable, accounting for their interdependencies. In our models, intrinsic neural timescales were the dependent variable, while the independent variables included the four visual indices and the baseline mean firing rate. To fit the linear model, we used robust regression, which minimizes the influence of outliers and is less sensitive to non-normality in the data. This approach ensures that the coefficients accurately reflect the effect of each predictor on the dependent variable without being disproportionately influenced by outliers. We utilized added-variable plots to illustrate the relationship between neural timescales and each predictor by plotting the controlled residuals against each independent variable (Figure 3A and 5B). These plots provide a visual representation of the distinct contributions of each predictor to the model, with the slopes quantifying the effect of a one-unit change in each predictor on the timescales while holding the other variables constant.

We checked for multicollinearity among the independent variables in the multiple regression model using Variance Inflation Factor (VIF) analysis. The VIF quantifies the degree to which the variance of a regression coefficient is inflated due to linear dependence on other predictors in the model. Generally, a VIF value greater than 5 or 10 suggests problematic multicollinearity (James et al., 2021), indicating that the affected predictors may be linearly dependent on others. In our analysis, we did not find significant multicollinearity, as shown in Figure S2A.

Additionally, we examined the normality of the residuals in our model. A Normal Q-Q plot was used to visually assess the distribution of residuals from our robust regression model against a theoretical normal distribution (Figure S2B). Deviations from the line in this plot indicate departures from normality, suggesting that the residuals were not normally distributed. To address this,

we used permutation testing to assess the significance of the regression coefficients. We employed a custom function to randomly shuffle the dependent variable, neural timescales, 10,000 times while keeping the independent variables unchanged. This generated a distribution of regression coefficients under the null hypothesis of no association (Figure 3A and 5B). P-values were calculated as the proportion of permuted coefficients whose absolute values equaled or exceeded that of the observed coefficient.

Neuron-dropping Decoding Analyses

To assess whether groups formed by shorter and longer intrinsic neural timescales differ in visual sensitivity and attentional responses at the population level, we conducted a neuron-decoding analysis (Lebedev, 2014). We tested the ability to decode spatial location (inside vs. outside the receptive field) during both transient and sustained stimulus presentations across single and pop-out trials. Neurons with fewer than 20 trials were excluded, resulting in 143 neurons in the shorter timescale group and 190 neurons in the longer timescale group.

To evaluate the decoding performance of varying neuron group sizes, we incrementally analyzed groups starting with three neurons and expanding up to 120 neurons. The maximum number of neurons was capped at 120 to avoid potential statistical validity issues that can arise when the subpopulation size approaches that of the fixed population (Lebedev, 2014). At each step, we randomly sampled the specified number of neurons 500 times to ensure robust performance estimates. For each decoding analysis (across 500 iterations at each step), we equalized the number of trials for In-RF and Out-RF conditions by randomly sampling an equal number of trials from each condition.

Next, we conducted principal component analysis (PCA), retaining the top three principal components after inspecting the scree plots. We then used a support vector machine (SVM) classifier for decoding. The decoding performances exhibited saturation curves as the number of neurons increased, indicating diminishing returns in performance improvement with additional neurons. To test whether the growth rates differed between shorter and longer timescale neurons, we fit a saturation function defined as:

$$f(x) = A \cdot e^{-B \cdot x} + C \tag{3}$$

Here, x represents the number of neurons ranging from 1 to 120, A represents the initial amplitude, B is the saturation rate, and C is the asymptote value of the function. To improve the fitting, we averaged the results of every five iterations, resulting in 100 averaged data points for each group over the incremental steps up to 120 neurons. We then fitted the saturation function to these 100 averaged iterations for each condition and computed the A, B, and C values. The parameters were compared between the shorter and longer timescale neurons using the nonparametric Wilcoxon rank-sum test. Additionally, we calculated confidence intervals for these parameters using bootstrapping to provide a measure of variability in our estimates.

Testing the Effect of Parietal Inactivation

To investigate the effects of parietal inactivation on intrinsic neural timescales, visual sensitivity, and attentional modulation in the FEF, we conducted a series of statistical analyses. First, we performed paired Wilcoxon signed-rank tests to determine whether parietal inactivation led to significant changes in FEF neural timescales, assessing the direction of change (increase or decrease) across both monkeys and within each individual monkey. The rank biserial correlation effect size was calculated to quantify the magnitude of the observed changes. Next, we analyzed whether the change (delta: inactivation - control) in neural timescales differed between

shorter and longer timescale neurons. We first tested against zero using a one-sample Wilcoxon signed-rank test to determine whether the change within each group was significant, followed by unpaired Wilcoxon rank-sum tests to compare the magnitude of change between the two groups.

We also examined whether the relationships between neural timescales and visual/attentional responses observed in the control condition persisted or were altered during inactivation. A multiple regression analysis was conducted using the same model as in the control condition, with intrinsic neural timescales as the dependent variable and visual indices along with baseline firing rate as independent variables. Changes in the distribution of visual and attentional indices were compared between shorter and longer timescale neurons. Additionally, we performed a neuron-dropping curve (NDC) analysis under inactivation to evaluate changes in visual and attentional decoding performance at the population level. The function parameters (saturation rate and asymptote value) were compared between shorter and longer timescale neurons in both conditions. Lastly, we analyzed the change in the area under the curve (AUC) above the chance level between control and inactivation using the trapezoidal rule.

Acknowledgments

This work was supported by the National Science Foundation National Research Traineeship (NSF NRT) under Grant No. 2152260 (to O.S.), National Institutes of Health grants EY014924 (to X.C.) and EY029759 (to T.M.), the Brain and Behavior Research Foundation (to X.C.), the Alfred P. Sloan Foundation under Grant No. FG-2021-16304 (to R.C.), and the UC Davis Large Interdisciplinary Applications in Neuroscience (LIAN) (to R.C. and X.C.).

Declaration of Interests

The authors declare no competing interests.

MAIN FIGURE TITLES AND LEGENDS

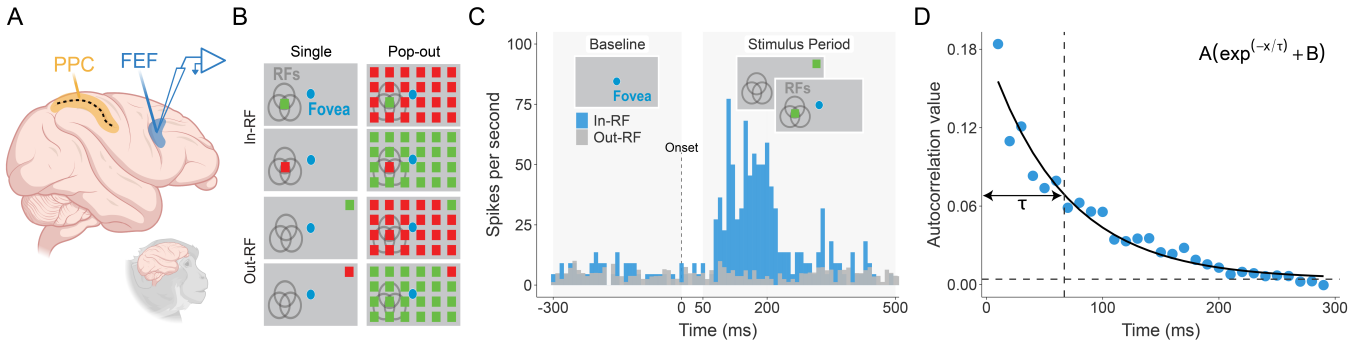

Figure 1. Experimental Setup and Intrinsic Neural Timescales

(A) FEF recordings were performed with a linear array with and without PPC inactivation. (B) Visual stimuli consisted of a single-colored stimulus presented in isolation (Single) or among an array of identically colored stimuli (Pop-out). (C) Mean response of an example neuron to a single stimulus presented inside (blue) versus outside (gray) the receptive field (RF). (D) Spike-count autocorrelation was computed for neuronal spiking activity during the baseline period. The decay of autocorrelation was fitted by an exponential decay with an offset. Solid lines show the exponential fit with the time constant (τ), indicating the intrinsic neural timescale.

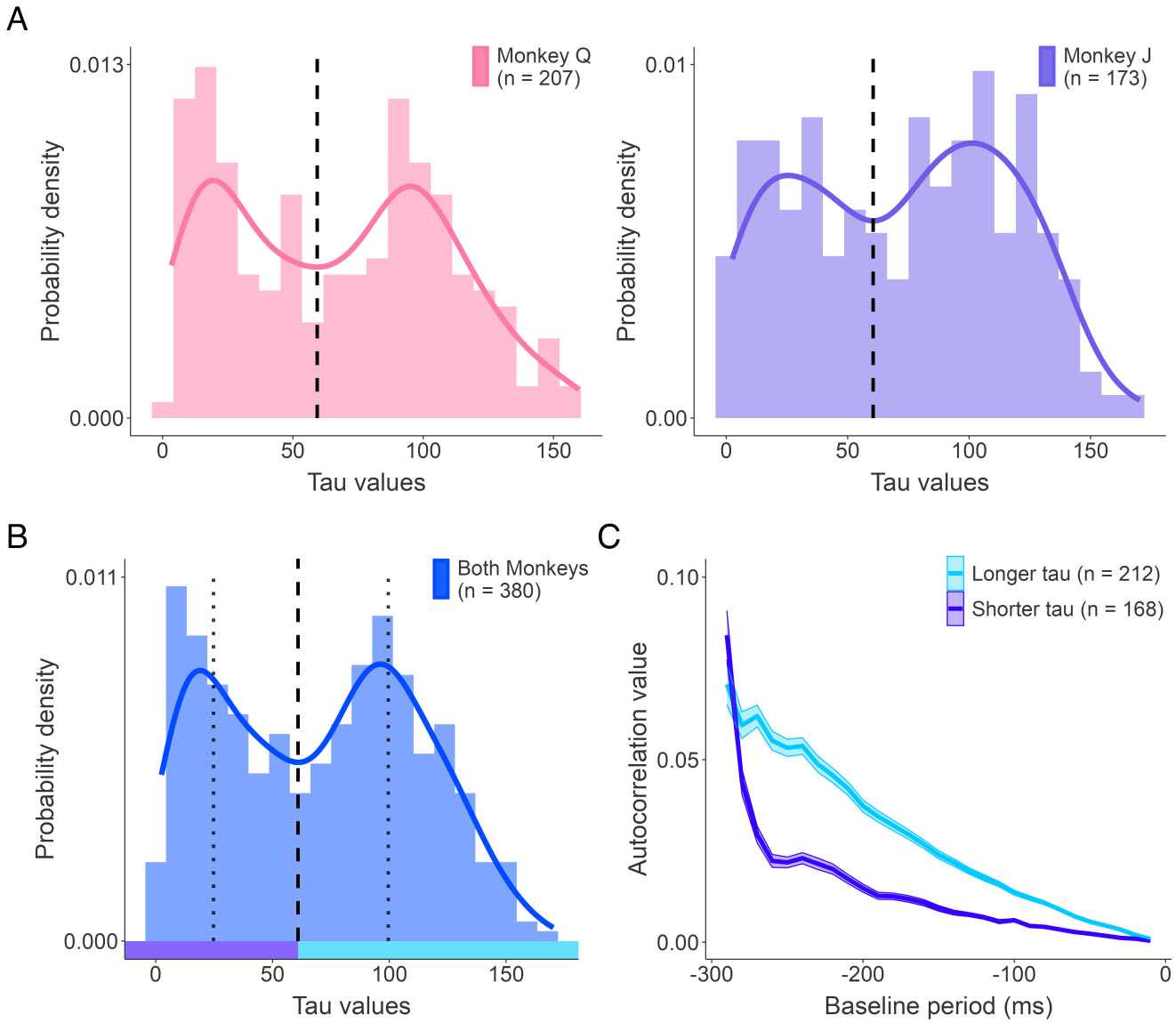

Figure 2. Distribution of Intrinsic Neural Timescales in FEF Neurons

(A) The distributions of intrinsic neural timescales (τ) were significantly bimodal for both monkeys. Solid lines represent the kernel density functions, while dashed lines indicate the global minima used to categorize neurons into shorter and longer timescale groups. (B) Distribution of τ values along with their kernel density plots across both monkeys. Dotted lines denote the median for each group. (C) Autocorrelation profiles for shorter and longer τ neurons during the baseline period.

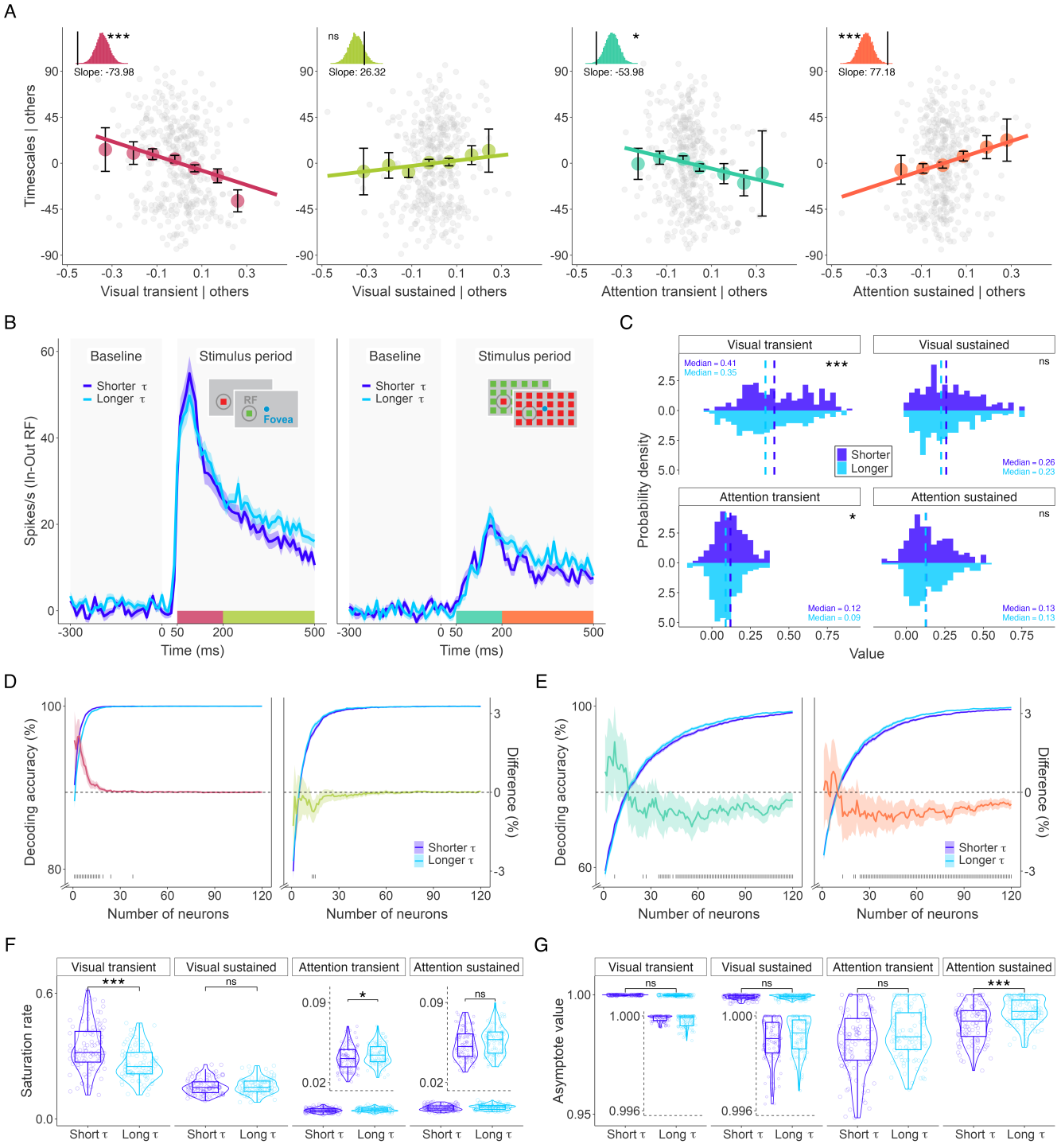

Figure 3. Relationship Between Intrinsic Neural Timescales and Functional Responses in FEF Neurons

Added-variable plots show the dependency between intrinsic neural timescales and visual (top) and attentional (bottom) responses. Insets display slopes and significance levels from the non-parametric permutation test. (B) Mean response difference between single (left) and unique (right) stimuli presented inside versus outside the receptive fields (In-RF vs. Out-RF) for shorter (purple) and longer τ neurons (blue). Shading around the response denotes $\pm$ SEM. (C) Distributions of visual and attention indices during the transient and sustained attention periods for shorter (purple) and longer τ neurons (blue). Dashed lines indicate the median value for each

group. (D) Population decoding performance for visual sensitivity as a function of population size of shorter (purple) and longer τ neurons (blue). Results are shown separately for the transient (left) and sustained (right) periods. Purple and blue lines represent average decoding accuracy, while other colored lines indicate the difference between the two groups. The black dashed line marks zero difference, and significant differences are indicated by gray vertical lines. Ribbons show 95% confidence intervals. (E) Population decoding performance for attentional modulation as a function of population size. Same conventions as in (D). (F) Boxplots comparing saturation rates of shorter and longer τ neurons across conditions. (G) Boxplots comparing asymptotic values of shorter and longer τ neurons across conditions. (*** $p < 0.001$, ** $p < 0.01$, * $p < 0.05$, ns = not significant).

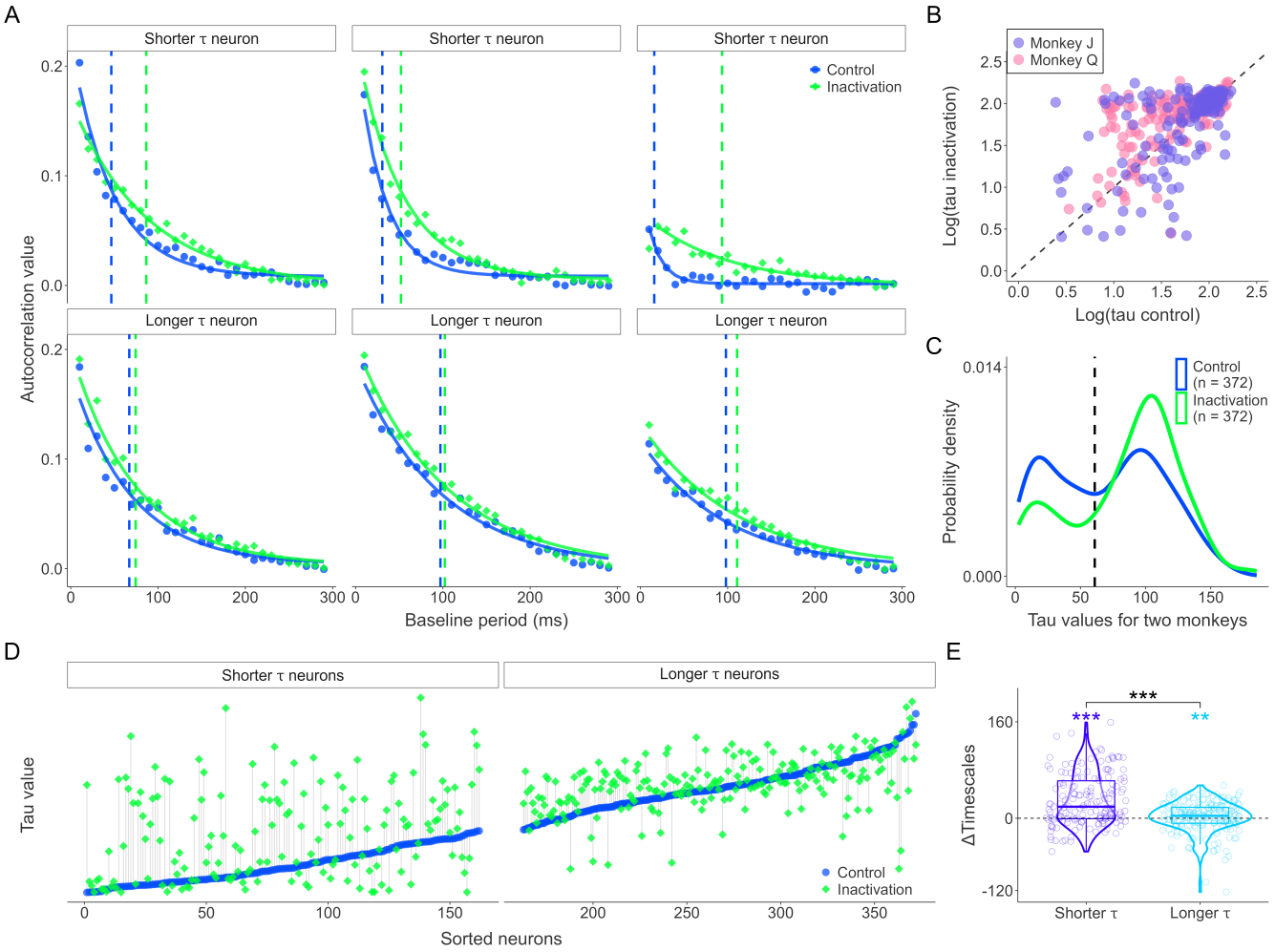

Figure 4. Effects of PPC Inactivation on Intrinsic Neural Timescales and Visual/Attentional Responses in the FEF

(A) Autocorrelation profiles of representative shorter τ neurons (top) and longer τ neurons (bottom) during control and PPC inactivation. Dashed lines indicate the timescale values for each condition. (B) Scatter plot of log-transformed timescale values for control vs. inactivation conditions for each monkey (Monkey J in purple, Monkey Q in pink). (C) Probability density plot of τ values for control (blue) and inactivation (green) conditions across two monkeys. (D) Sorted timescale values for shorter and longer τ neurons in control and inactivation conditions. (E) Violin plots comparing the change in timescale values between control and inactivation conditions for shorter and longer τ neurons. (*** $p < 0.001$, ** $p < 0.01$, * $p < 0.05$, ns = not significant).

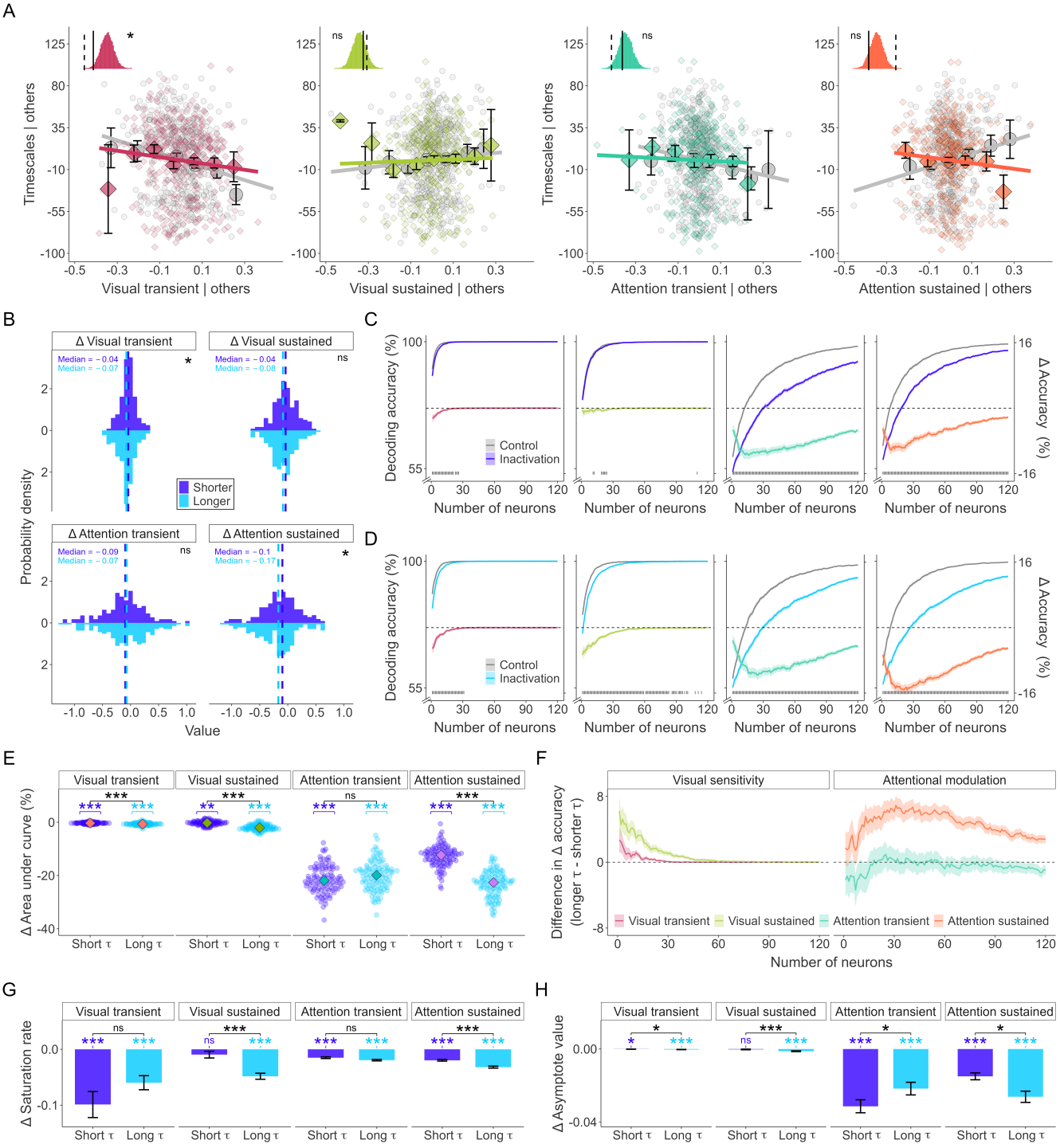

Figure 5. Effects of PPC Inactivation on Visual and Attentional Processing in FEF Neurons

(A) Added-variable plots showing the relationship between τ and visual/attentional responses before and after PPC inactivation. Insets display slopes and significance from permutation tests. (B) Changes in the distributions of visual and attention indices for shorter (purple) and longer τ neurons (blue) following PPC inactivation. Dashed lines show median changes for each group. (C) Visual and attention decoding performance as a function of population size after PPC inactivation for shorter τ neurons. Gray and purple lines represent inactivation and control, with differences shown on the secondary axis and significant differences marked by gray vertical

lines. (D) Same as (C), but for longer τ neurons, with gray and blue lines. (E) AUC changes from neural dropping curves (NDCs) for shorter and longer τ neurons after PPC inactivation. (F) Difference in the changes in decoding performance from control to inactivation for shorter and longer τ neurons. Positive y-axis values indicate larger changes for longer τ neurons, while negative values indicate larger changes for shorter τ neurons. (G) Violin plots comparing saturation rates between shorter and longer τ neurons after PPC inactivation. (H) Violin plots comparing asymptotic values between shorter and longer τ neurons after PPC inactivation. (*** $p < 0.001$, ** $p < 0.01$, * $p < 0.05$, ns = not significant).

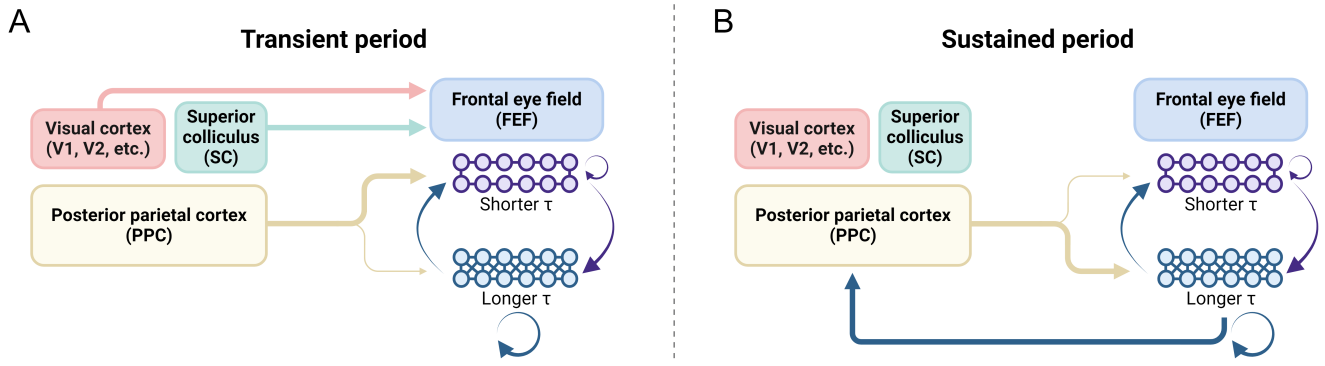

Figure 6. Possible Intra- and Inter-area Communication Between PPC and FEF During Stimulus-driven Attention

(A) During the transient attention period, rapid attentional responses are primarily driven by feedforward projections from the PPC to shorter τ neurons in the FEF. (B) During the sustained attention period, the maintenance of attentional information is driven by reciprocal connections between the PPC and longer τ neurons in the FEF. The attentional response of longer τ neurons is initially driven by shorter τ neurons and subsequently maintained over a longer period through recurrent local and long-range connections. As a result, PPC inactivation led to a significant reduction in the attentional response of longer τ neurons.

References

Ameijeiras-Alonso, J., Crujeiras, R. M., and Rodriguez-Casal, A. (2021). multimode: An R Package for Mode Assessment. *Journal of Statistical Software*, 97:1–32.

Ameijeiras-Alonso, J., Crujeiras, R. M., and Rodríguez-Casal, A. (2019). Mode testing, critical bandwidth and excess mass. *TEST*, 28(3):900–919.

Boshra, R. and Kastner, S. (2022). Attention control in the primate brain. *Current Opinion in Neurobiology*, 76:102605.

Bruce, C. J., Goldberg, M. E., Bushnell, M. C., and Stanton, G. B. (1985). Primate frontal eye fields. II. Physiological and anatomical correlates of electrically evoked eye movements. *Journal of Neurophysiology*, 54(3):714–734. Publisher: American Physiological Society.

Cavanagh, S. E., Hunt, L. T., and Kennerley, S. W. (2020). A Diversity of Intrinsic Timescales Underlie Neural Computations. *Frontiers in Neural Circuits*, 14. Publisher: Frontiers.

Cavanagh, S. E., Wallis, J. D., Kennerley, S. W., and Hunt, L. T. (2016). Autocorrelation structure at rest predicts value correlates of single neurons during reward-guided choice. *eLife*, 5:e18937. Publisher: eLife Sciences Publications, Ltd.

Chaudhuri, R., Bernacchia, A., and Wang, X.-J. (2014). A diversity of localized timescales in network activity. *eLife*, 3:e01239. Publisher: eLife Sciences Publications, Ltd.

Chaudhuri, R., Knoblauch, K., Gariel, M.-A., Kennedy, H., and Wang, X.-J. (2015). A Large-Scale Circuit Mechanism for Hierarchical Dynamical Processing in the Primate Cortex. *Neuron*, 88(2):419–431. Publisher: Elsevier.

Chen, X., Zirnsak, M., Vega, G. M., Govil, E., Lomber, S. G., and Moore, T. (2020). Parietal Cortex Regulates Visual Salience and Salience-Driven Behavior. *Neuron*, 106(1):177–187.e4.

Demirtaş, M., Burt, J. B., Helmer, M., Ji, J. L., Adkinson, B. D., Glasser, M. F., Van Essen, D. C., Sotiropoulos, S. N., Anticevic, A., and Murray, J. D. (2019). Hierarchical Heterogeneity across Human Cortex Shapes Large-Scale Neural Dynamics. *Neuron*, 101(6):1181–1194.e13.

Elston, G., Benavides-Piccione, R., Elston, A., Manger, P., and Defelipe, J. (2011). Pyramidal Cells in Prefrontal Cortex of Primates: Marked Differences in Neuronal Structure Among Species. *Frontiers in Neuroanatomy*, 5.

Elston, G. N. (2000). Pyramidal Cells of the Frontal Lobe: All the More Spinous to Think With. *Journal of Neuroscience*, 20(18):RC95–RC95. Publisher: Society for Neuroscience Section: RAPID COMMUNICATION.

Elston, G. N. (2003). Cortex, cognition and the cell: new insights into the pyramidal neuron and prefrontal function. *Cerebral Cortex (New York, N.Y.: 1991)*, 13(11):1124–1138.

Fallon, J., Ward, P. G. D., Parkes, L., Oldham, S., Arnatkevičiūtė, A., Fornito, A., and Fulcher, B. D. (2020). Timescales of spontaneous fMRI fluctuations relate to structural connectivity in the brain. *Network Neuroscience*, 4(3):788–806.

Fisher, N. I. and Marron, J. S. (2001). Mode testing via the excess mass estimate. *Biometrika*, 88(2):499–517.

Gao, R., van den Brink, R. L., Pfeffer, T., and Voytek, B. (2020). Neuronal timescales are functionally dynamic and shaped by cortical microarchitecture. *eLife*, 9:e61277. Publisher: eLife Sciences Publications, Ltd.

Hall, P. and York, M. (2001). On the Calibration of Silverman's Test for Multimodality. *Statistica Sinica*, 11(2):515–536. Publisher: Institute of Statistical Science, Academia Sinica.

Hart, E. and Huk, A. C. (2020). Recurrent circuit dynamics underlie persistent activity in the macaque frontoparietal network. *eLife*, 9:e52460. Publisher: eLife Sciences Publications, Ltd.

Hartigan, J. A. and Hartigan, P. M. (1985). The Dip Test of Unimodality. *The Annals of Statistics*, 13(1):70–84. Publisher: Institute of Mathematical Statistics.

Hasson, U., Chen, J., and Honey, C. J. (2015). Hierarchical process memory: memory as an integral component of information processing. *Trends in cognitive sciences*, 19(6):304–313.

James, G., Witten, D., Hastie, T., and Tibshirani, R. (2021). Linear Regression. In James, G., Witten, D., Hastie, T., and Tibshirani, R., editors, *An Introduction to Statistical Learning: with Applications in R*, pages 59–128. Springer US, New York, NY.

Lebedev, M. A. (2014). How to read neuron-dropping curves? *Frontiers in Systems Neuroscience*, 8:102.

Litwin-Kumar, A. and Doiron, B. (2012). Slow dynamics and high variability in balanced cortical networks with clustered connections. *Nature Neuroscience*, 15(11):1498–1505.

Lomber, S. G. and Payne, B. R. (2000). Translaminar differentiation of visually guided behaviors revealed by restricted cerebral cooling deactivation. *Cerebral Cortex (New York, N.Y.: 1991)*, 10(11):1066–1077.

Lynch, J. C. and Tian, J.-R. (2006). Cortico-cortical networks and cortico-subcortical loops for the higher control of eye movements. *Progress in Brain Research*, 151:461–501.

Markov, N. T., Misery, P., Falchier, A., Lamy, C., Vezoli, J., Quilodran, R., Gariel, M. A., Giroud, P., Ercsey-Ravasz, M., Pilaz, L. J., Huissoud, C., Barone, P., Dehay, C., Toroczkai, Z., Van Essen, D. C., Kennedy, H., and Knoblauch, K. (2011). Weight consistency specifies regularities of macaque cortical networks. *Cerebral Cortex (New York, N.Y.: 1991)*, 21(6):1254–1272.

Moore, T. and Armstrong, K. M. (2003). Selective gating of visual signals by microstimulation of frontal cortex. *Nature*, 421(6921):370–373. Publisher: Nature Publishing Group.

Moore, T. and Fallah, M. (2001). Control of eye movements and spatial attention. *Proceedings of the National Academy of Sciences of the United States of America*, 98(3):1273–1276.

Moore, T. and Zirnsak, M. (2017). Neural Mechanisms of Selective Visual Attention. *Annual Review of Psychology*, 68(Volume 68, 2017):47–72. Publisher: Annual Reviews.

Murray, J. D., Bernacchia, A., Freedman, D. J., Romo, R., Wallis, J. D., Cai, X., Padoa-Schioppa, C., Pasternak, T., Seo, H., Lee, D., and Wang, X.-J. (2014). A hierarchy of intrinsic timescales across primate cortex. *Nature Neuroscience*, 17(12):1661–1663. Number: 12 Publisher: Nature Publishing Group.

Murray, J. D., Jaramillo, J., and Wang, X.-J. (2017). Working Memory and Decision-Making in a Frontoparietal Circuit Model. *Journal of Neuroscience*, 37(50):12167–12186. Publisher: Society for Neuroscience Section: Research Articles.

Pettine, W. W., Steinmetz, N. A., and Moore, T. (2019). Laminar segregation of sensory coding and behavioral readout in macaque V4. *Proceedings of the National Academy of Sciences*, 116(29):14749–14754. Publisher: Proceedings of the National Academy of Sciences.

Schall, J. D., Morel, A., King, D. J., and Bullier, J. (1995). Topography of visual cortex connections with frontal eye field in macaque: convergence and segregation of processing streams. *The Journal of Neuroscience: The Official Journal of the Society for Neuroscience*, 15(6):4464–4487.

Stanton, G. B., Bruce, C. J., and Goldberg, M. E. (1995). Topography of projections to posterior cortical areas from the macaque frontal eye fields. *Journal of Comparative Neurology*, 353(2):291–305. _eprint: https://onlinelibrary.wiley.com/doi/pdf/10.1002/cne.903530210.

Wang, X.-J. (2020). Macroscopic gradients of synaptic excitation and inhibition in the neocortex. *Nature Reviews. Neuroscience*, 21(3):169–178.

Wasmuht, D. F., Spaak, E., Buschman, T. J., Miller, E. K., and Stokes, M. G. (2018). Intrinsic neuronal dynamics predict distinct functional roles during working memory. *Nature Communications*, 9(1):3499. Number: 1 Publisher: Nature Publishing Group.

Wessberg, J., Stambaugh, C. R., Kralik, J. D., Beck, P. D., Laubach, M., Chapin, J. K., Kim, J., Biggs, S. J., Srinivasan, M. A., and Nicolelis, M. A. L. (2000). Real-time prediction of hand trajectory by ensembles of cortical neurons in primates. *Nature*, 408(6810):361–365. Publisher: Nature Publishing Group.

Wolff, A., Berberian, N., Golesorkhi, M., Gomez-Pilar, J., Zilio, F., and Northoff, G. (2022). Intrinsic neural timescales: temporal integration and segregation. *Trends in Cognitive Sciences*, 26(2):159–173.

Zeraati, R., Shi, Y.-L., Steinmetz, N. A., Gieselmann, M. A., Thiele, A., Moore, T., Levina, A., and Engel, T. A. (2023). Intrinsic timescales in the visual cortex change with selective attention and reflect spatial connectivity. *Nature Communications*, 14(1):1858. Number: 1 Publisher: Nature Publishing Group.